Anal Bioanal Chem (2009) 395:171–184
DOI 10.1007/s00216-009-2938-y

ORIGINAL PAPER

Matisse to Picasso: a compositional study of modern bronze sculptures

Marcus L. Young · Suzanne Schnepp · Francesca Casadio · Andrew Lins · Melissa Meighan · Joseph B. Lambert · David C. Dunand

Received: 8 February 2009 / Revised: 6 June 2009 / Accepted: 25 June 2009 / Published online: 23 July 2009

Abstract Inductively coupled plasma-optical emission spectroscopy (ICP-OES) was used to determine the bulk metal elemental composition of 62 modern bronze sculptures cast in Paris in the first half of the twentieth century from the collections of The Art Institute of Chicago and the Philadelphia Museum of Art. As a result, a comprehensive survey of the alloy composition of the sculptures of many prominent European artists of the early twentieth century is presented here for the first time. The sculptures in this study consist of predominantly copper with two main alloying elements (zinc and tin). By plotting the concentrations of these two elements (zinc and tin) against each other for all the sculptures studied, three clusters of data become apparent: (A) high-zinc brass; (B) low-zinc brass; (C) tin bronze. These clusters correlate to specific foundries, which used specific casting methods (sand or lost wax) that were influenced by individual preferences and technical skills of the foundry masters. For instance, the high-zinc brass alloys (with the highest levels of tin and zinc and the lowest melting temperature) correspond to most of the Picasso sculptures, correlate with the Valsuani foundry, and are associated with the most recent sculptures (post-WWII) and with the lost-wax casting method. By expanding the ICP-OES database of objects studied, these material correlations may become useful for identifying, dating, or possibly even authenticating other bronzes that do not bear foundry marks.

Keywords Bronze sculpture · ICP-OES · Modern bronze

Electronic supplementary material The online version of this article (doi:10.1007/s00216-009-2938-y) contains supplementary material, which is available to authorized users.

M. L. Young · D. C. Dunand
Department of Materials Science and Engineering,
Northwestern University,
Evanston, IL 60208, USA

S. Schnepp · F. Casadio (✉)
The Art Institute of Chicago,
Chicago, IL 60603, USA
e-mail: fcasadio@artic.edu

A. Lins · M. Meighan
The Philadelphia Museum of Art,
Philadelphia, PA 19101, USA

J. B. Lambert
Department of Chemistry, Northwestern University,
Evanston, IL 60208, USA

Introduction

Many of the bronze sculptures produced by European masters of the first half of the twentieth century were cast in the Parisian foundries that had brought the art of sand and lost-wax casting to a very high level. The resulting sculptures vary greatly in appearance ranging from highly polished metal surfaces to heavily patinated surfaces. The foundries of the period were quite secretive about their alloys (and patination solutions) used in order to prevent other foundries from producing a superior product, which suggests that alloy composition may be sufficient to identify which foundry cast a particular sculpture. This would be advantageous because not all the sculptures bear a foundry mark or have documentary evidence to identify in which of the many Parisian art foundries they were cast.

Importance of alloying additions to copper

Bronze composition is relevant for the artist who cares about the color of the metal and patina and for the foundryman for whom composition determines alloy cost, castability, shrinkage, and casting method. For instance, the

addition of small amounts of tin (1–6 wt.%) to copper effectively lowers the melting temperature required for casting. Besides improving the castability of the alloy, adding tin has the benefit of making sculptures harder, stronger, and more corrosion/oxidation resistant than copper alone. Similarly, the addition of zinc (1–35 wt.%) to copper also lowers the melting temperature for casting, but, on a weight basis, Zn is less efficient than Sn at depressing the liquidus of copper [1]. Zinc additions also make copper harder, stronger, and more corrosion/oxidation resistant. However, above about 15 wt.% Zn, the alloy becomes susceptible to dezincification, a condition resulting in selective removal of zinc in the presence of oxygen and water, which leaves behind a porous, copper-rich surface. Adding small amounts of tin to a copper–zinc alloy greatly increases its resistance to dezincification [2]. Alloying additions also affect the color of the copper. As the amount of tin increases from 1 to 6 wt.%, the metal color changes from a dark reddish brown (copper color) to a light gold color. With additions of zinc (1–35 wt.%), the copper color shifts to a light silvery color. Besides affecting the appearance of the base metal, alloying also affects the patination. These alloys react differently to a given chemical patination solution and, therefore, result in a different appearance. For example, increasing the amount of Sn makes patination easier, but the final step of chiseling or punching ("chasing") the sculpture becomes more difficult [3]. This is particularly relevant for sand cast sculptures, which require a lot of hand finishing. An in-depth knowledge of bronze composition can thus become an element of secondary evidence for the art historian and connoisseur studying early twentieth century sculpture and trying to address questions about authenticity, provenance, and artist intention.

A note on traditional casting methods

Sand and lost-wax casting were the methods of choice for the art foundries of early twentieth century France. These complex processes of sculpture manufacturing generally leave behind some traces, which aid in visually identifying the casting method used for a particular sculpture.

Sand casting typically begins with a plaster model set into a two-part or multipart casting flask [3–5]. In each part, the plaster is surrounded by packed sand. After the flask is opened, the plaster model is removed and replaced with a core composed of fine sand and other materials, often including iron wire or rod. This core, which is roughly 1–2 cm. smaller than the plaster original, is held in place in the void previously occupied by the plaster model with pins (chaplets) that extend into the adjacent sand and leave equal spacing around the core. This space or gap is filled by molten metal during the casting. In larger sand castings, appendages such as heads and outstretched arms or legs are often cast separately and joined, usually mechanically, to other sections. This technique requires great skills in mold design and construction and in the assembly of the sections. The finishing steps in the best castings disguise the joints very successfully and usually entail extensive hammering/planishing [6].

Although the lost-wax method is ancient, dating back to as early as 3600 BC in the Middle East [4, 7, 8], it was rarely used in France by the early nineteenth century, when most artists and foundries were using the sand casting method [3, 4]. Lost-wax casting in the twentieth century involved using a flexible (gelatin or, later, agar or rubber) mold to take an impression of a model [4]. This impression was then coated with a wax layer in the interior. The cavity was filled with a plaster-based material to create the core. This wax-surfaced "positive" could be easily adjusted by the artist by adding or subtracting wax at this stage. Pouring channels and vents were then created from wax, and the whole sculpture was encased in a plaster-based "retainer" mold. The mold was heated to melt out the wax, and the bronze was poured. The sculpture could usually easily be cast all in one piece, thus obviating the need for the assembling workman and for extensive surface work to remove mold lines resulting from the sand casting method. Lost-wax casting also had the reputation of being better at reproducing fine detail, though the best sand cast pieces could display excellent detail as well. In the first half of the twentieth century, artists gradually converted from sand to lost-wax casting due to the development of limited editions, ease of repair/alteration of the wax model, and the reproducibility of fine detail.

While some foundries started with the sand casting method and then switched to the lost-wax casting method as it gained in popularity during this period, many foundries used only the sand (i.e., Rudier) or lost-wax (i.e., Hébrard) casting method exclusively [3].

Scientific studies of artistic bronzes

Scientific studies of modern art materials have predominately focused on the study of modern paints [9–12], polymers used in modern textiles [13], and other plastic artifacts [14]. For modern bronzes and three-dimensional works in other media, the focus in the literature has rather been on their conservation [15–17]. To date, only a small number of papers have examined modern artistic metals using inductively coupled plasma (ICP) spectroscopy [18, 19], X-ray fluorescence (XRF) [4], or scanning electron microcopy/energy-dispersive X-ray spectroscopy (EDX) [4, 19, 20], focusing mostly on the studio practices of Henri Matisse [4, 18] and Auguste Rodin [20].

Rather than concentrating on one case study or devoting a monographic effort on a single artist, the research presented here examines, for the first time, a large number of sculptures representing many different artists and foundries. Sixty-two modern bronzes—from the collections of The Art Institute of Chicago (AIC, 46 sculptures) and the Philadelphia Museum of Art (PMA, 16 sculptures)—were examined primarily using ICP-optical emission spectroscopy (ICP-OES) to determine the precise elemental composition of the alloys. These modern bronzes, dating from the 1900s to the 1950s, include sculptures by many prominent artists of the time, such as Joseph Antoine Bernard, Pierre Bonnard, Marcel Bouraine, Emile Antoine Bourdelle, Constantin Brancusi, Charles Despiau, Raymond Duchamp-Villon, Guitou Knoop, Paul Landowski, Jacques Lipchitz, Aristide Maillol, Henri Matisse, Chana Orloff, Pablo Picasso, Jane Poupelet, Pierre-Auguste Renoir, Auguste Rodin, and Ossip Zadkine (see Table 1). In addition to these modern bronze sculptures, eight commercially available bronze standards and reference materials were examined for comparison and to calibrate and validate the analytical approach.

ICP-OES and ICP-mass spectrometry (MS) have been shown to be effective tools in the study of ancient Cu-based artifacts [18, 21–27]. The widespread availability of the equipment (as opposed to, for example, neutron activation analysis or electron microprobe analysis), very wide range of measurable elements, and good sensitivity (higher than, for instance, atomic absorption spectroscopy and X-ray fluorescence) make ICP-OES and ICP-MS very useful elemental analysis techniques for these studies. Although ICP-OES and ICP-MS techniques are destructive, they require only a very small amount of material (~10 mg), which can be taken from a discreet area on the sculpture (preferably at the base or another location hidden from view) and thus can provide very accurate local detail about the elemental composition.

The overarching goal of the present study is to provide material data and correlations of art historical significance between compositional results and the artist, the foundry, the casting method, and the date of creation and casting, thus providing material and historical context for these sculptures. By expanding the current data set, this research may assist in the attribution and dating of some of the sculptures.

Experimental procedures

ICP-OES was performed using a Varian model ICP spectrometer with spectral range from 175 to 785 nm and resolutions of 0.008, 0.015, and 0.040 nm at 160–335, 335–670, and 670–850 nm, respectively. Qualitative ICP-MS was performed in select cases with a VG Elemental PQ-ExCell quadrupole ICP-MS with collision cell. Additionally, preliminary XRF measurements were also conducted in order to confirm that the area chosen for sampling was representative of the general composition of the alloy of the sculptures, as well as to determine the composition of reference metals and ICP-OES standards to acquire for this study. The XRF measurements were performed with a portable Bruker Tracer III-V energy-dispersive X-ray fluorescence spectrometer with an X-ray tube equipped with a rhodium (Rh) transmission target and thermoelectrically cooled Ag-free SiPIN detector. Discussion of the results of the XRF study and their comparison with ICP-OES results are beyond the scope of this study and will be the subject of a separate publication.

Samples from the modern bronze sculptures were obtained by drilling small 1.6-mm-diameter holes with cobalt steel drill bits in discreet areas, such as the underside of the sculpture base. The holes were drilled initially to a depth of approximately 1 mm and the turnings were discarded to avoid collecting samples with oxidation, corrosion products, or other extraneous deposits and to ensure that only bulk material was collected. Then, the hole was further drilled until approximately 10 mg of bulk alloy was collected. Although necessary for sampling for ICP-OES, it should be noted here that the use of drill bits may result in a slight increase, for example, in the measured wt. % of Fe, which contributes to a constant background and does not create differences from sample to sample. Additional reference samples from commercial bronzes (SiPi Metals Corporation (SIPI) and Atlas Bronze) and National Institute of Standards and Technology standards with similar compositions to the modern bronzes were also collected using the same methodology (see Supporting Information ESM 1).

Each sample was weighed (measuring on average 10 mg) and placed in a 10-mL conical polypropylene tube with 1.0 mL of aqua regia (75% (*v*/*v*) HCl–25% (*v*/*v*) HNO_3) and left for 24 h for complete dissolution. After dissolution, the samples were further diluted with aqua regia and ultrapure Millipore H_2O to reach solutions of approximate concentrations of 5, 10, 20, 100, and 200 μg/mL in ~3% (*v*/*v*) aqua regia. To each dilution, 1 μg/mL of Eu was added as an internal normalization standard for ICP-OES. Eu was selected due to its large isolated emission lines at 420 and 443 nm as compared to the other elements present in the bronzes. In addition, two sets of ICP-OES standards were created (one with As, Sb, and Sn in 3% (*v*/*v*) HCl: the other with Bi, Cr, Cu, Fe, Ni, Pb, and Zn in 3% (*v*/*v*) HNO_3) with all standard solutions containing 1 μg/mL of Eu as an internal normalization standard. All single-element (As, Sb, Sn, Bi, Cr, Cu, Fe, Ni, Pb, Zn, and Eu) starting solutions before dilution were purchased from either

Table 1 Description of 62 modern bronzes studied here, including artist, accession number (AIC and PMA indicate the sculpture is from the collection of The Art Institute of Chicago and the Philadelphia Museum of Art, respectively), title, foundry, casting method, date of creation, date of casting, and corresponding cluster (A, B, and C)

Artist	Accession #	Title	Foundry	Casting method	Creation date	Casting date	Cluster
Bernard	AIC: 1943.1189	Girl with Pail	Hébrard	Lost wax	1910		A
Bonnard	AIC: 1963.927	Spring Frolic			1904–1906		A
Bouraine	AIC: 1973.774	Dancing Woman with Hoop			1925–1935		
Bourdelle	AIC: 1997.543[a]	Head of Apollo	Alexis Rudier	Sand	1900		C
	AIC: 1950.141	Head of Young Woman	Alexis Rudier	Sand	c. 1910		C
	AIC: 1925.255[a]	Heracles (Archer)	Alexis Rudier	Sand	1909	1920–1922	C
	AIC: 1953.168	Penelope		Sand	1911		
Brancusi	PMA: 1967.30.6a,b	Danaide	C. Valsuani	Lost wax	1913	1920	A
	AIC: 1985.542a,b[a]	Suffering	C. Valsuani	Lost wax	Pre-1907	1907	A
Daumier	PMA: 1957.127.11a,b	Alexandre-Simon Pataille	Barbedienne	(Sand)	c. 1932	c. 1955	
	PMA: 1986.26.275	L'Obsequieux	Barbedienne: M.L.G.[b]				
	PMA: 1986.26.9a,b	Ratapoil	Alexis Rudier		Pre-1925	c. 1925	C
Degas	PMA: 1954.92.21a,b	Woman Rubbing her Back with a Sponge, Torso	Hébrard	Lost wax		Post-1920	A
	PMA: 1963.181.82a,b	Woman Taken Unawares	Hébrard	Lost wax		Post-1920	A
Despiau	AIC: 1954.324	Madame de Waroquier	C. Valsuani	Lost wax	1927		A
	AIC: 1950.93	Young Girl	C. Valsuani	Lost wax	1929		A
Duchamp-Villon	AIC: 1957.165	Horse	Susse		1914	1955–1957	
Knoop	AIC: 1939.238	Katharine Cornell	C. Valsuani	Lost wax	1937		A
Landowski	AIC: 1923.314	Henry Harrison Getty	C. Valsuani	Lost wax	1918		
Lipchitz	AIC: 1996.394	Mother and Child			1949		
	AIC: 1943.594	Rape of Europa			1938		
	AIC: 1955.826	The Reader		Lost wax	1919		
	PMA: 1949.78.1a,b	Sailor with Guitar	C. Valsuani		1914		
	PMA: 1955.96.2a,b	Woman with Braid	C. Valsuani	Lost wax	1914		
Maillol	AIC: 1934.383[a]	Girl with Arm over Her Eyes		Sand	1900		B
	AIC: 1947.86	Leda		Sand	c. 1902		B
	PMA: 1950.92.44	Leda	Alexis Rudier		c. 1900		
	AIC: 1934.384	Nude		(Sand)	1900		B
	AIC: 1932.1144a,b	Renoir		(Sand)	1907		B
	AIC: 1971.779	Woman with Crab			1903		B
Matisse	AIC: 1958.16	Seated Nude	C. Valsuani	Lost wax	c. 1922–1925	1951	A
	PMA: 1960.146.1a,b	Seated Nude with Pedestal	C. Valsuani	Lost wax	c. 1925		A
	AIC: 1949.202a,b	The Serf	Bingen-Costenoble	(Sand)	Pre-1908	1908	B
	PMA: 1963.210a,b	Serpentine Woman	C. Valsuani	Lost wax	1909		A

Table 1 (continued)

Artist	Accession #	Title	Foundry	Casting method	Creation date	Casting date	Cluster
	PMA: 1967.030.51a,b	Standing Nude with Arms Raised	Bingen-Costenoble		1906		B
	AIC: 1992.654	Woman Leaning on Her Hands	(C. Valsuani)	Lost wax	1905	c. 1930	A
	AIC: 1932.1145	Small Crouching Nude without an Arm	(F. Godard)	(Sand)	c. 1908	1922–1923	B
Orloff	AIC: 1930.227	Woman with Basket	Alexis Rudier	Sand	1926		C
Picasso	AIC: 1967.682	Female Figure	C. Valsuani	Lost wax	1945–1947		B
	AIC: 1957.70a, b[a]	Flowers in a Vase	C. Valsuani	Lost wax	1951	1953	A
	AIC: 1949.584	Head of a Woman (Fernande)		Sand	1909	1909–1912	
	AIC: 1964.193	Jester		Sand	1905		B
	AIC: 1967.683	Standing Woman 1		(Lost wax)	1947		A
	AIC: 1967.685	Standing Woman 2	C. Valsuani	Lost wax	1947		A
	AIC: 1967.686	Standing Woman 3		(Lost wax)	1945		A
	AIC: 1967.687	Standing Woman 4	C. Valsuani	Lost wax	1947		A
	AIC: 1967.688	Standing Woman 5		(Lost wax)	1945		A
	AIC: 1967.689	Standing Woman 6	C. Valsuani	Lost wax	1947		A
	AIC: 1967.690	Standing Woman 7		Lost wax	1945		A
Poupelet	AIC: 1927.366	Cat		Sand	Pre-1924	Pre-1924	B
	AIC: 1931.569	Cat	L. Gatti	Lost wax	Pre-1931	Pre-1931	
	AIC: 1927.368	Cock		(Sand)	1909	Pre-1927	C
	AIC: 1927.365.2	Cow		Sand	1900–1910		B
	AIC: 1931.568	Goat		(Sand)	Pre-1931	Pre-1931	B
	AIC: 1927.369	Goose		(Sand)	1909		A
	AIC: 1927.365.1	Peasant		Sand	1900–1910		C
	AIC: 1927.367	Rabbit		Sand	1909		B
	AIC: 1927.364	Woman Bathing		Sand	1900–1910		B
Renoir	PMA: 1950.92.47a,b	Head of Coco	C. Valsuani		1908		A
Rodin	PMA: 1967.30.73a,b	The Athlete			Pre-1904	1904	C
	PMA: 1929.7.4a,b	The Athlete	Alexis Rudier		Pre-1925	1925	C
Zadkine	PMA: 1964.80.1a,b	Harlequin	Grandhomme-Andro		1928		

Unknown information is left blank. In the "Foundry" and "Casting method" columns, parentheses indicate value is likely (as inferred by visual observation and available information) but not known. Measurements from two different sites on the same sculpture are designated by a and b at the end of the accession #

[a] ICP-MS was also performed

[b] M.L.G. refers to the owner (Maurice Le Garrec) of the original clay models from which the bronze casts were made, and indicated his authorization of the casting

Aldrich or Fluka chemical companies. Both sets of ICP-OES standards were measured before testing the unknown modern bronzes to produce a best-fit curve based on three replications at each concentration for each selected element. Intensity of selected emission lines of the elements of interest vs. concentration using a blank (0 μg/mL), which consisted of 3% (*v*/*v*) HNO_3, was used for background subtraction. Five concentrations (0.1, 0.5, 1, 5, 10, and 25 μg/mL) from each set of ICP-OES standards were used to generate calibration curves, which were then used to estimate elemental concentrations based on intensity of emission of an unknown modern bronze sample.

After all of the calibration curves for the ICP-OES standard were generated, the known commercial bronzes and unknown modern bronzes were analyzed. Generally, the concentrations of the elements falling in the compositional range of 55–100 wt.% (i.e., Cu) were determined from the 10-μg/mL sample dilution. The concentrations of the elements in the compositional range of 12–55 wt.% (i.e., Zn) were determined from the 20-μg/mL sample dilution. The concentrations of the elements in the compositional range of 6–12 wt.% (i.e., Sn and Zn) were determined from the 100-μg/mL sample dilution. The concentrations of the elements in the compositional range of 0.1–6 wt.% were determined from the 200-μg/mL sample dilution. Instrument detection limits in microgram per milliliter for specific emission lines from each element are shown in ESM 1.

Results and discussion

Elemental compositions before normalization for the as-received standards and references as reported by the manufacturer and values determined by ICP-OES in this experiment are shown in totality in Supporting Information ESM 1 and for two selected modern bronzes in Table 2. In all tables and throughout the rest of this paper, all compositions are expressed in weight percent. Replicate analysis of the reference metals and standards highlighted that the error on the commercial bronzes can be calculated to 1% of the reported values, indicating good accuracy of the method and also that it is possible to use the commercial references from SIPI metals and Atlas for validating modern bronze measurements.

Table 3 presents elemental compositions and their standard deviations determined from ICP-OES for all modern bronzes studied, after normalization (for details about normalization, see Note on Experimental Error and Normalization Factors in Supporting Information). Each set of elemental wavelength measurements is multiplied by a specific normalization factor.

Additional trace elements are most probably present but were not measured specifically by ICP-OES here. To address this issue, qualitative ICP-MS analysis, which provides the entire elemental spectrum and thus allows for the identification of all elements present [28–30], was performed on a select number of commercial and modern bronzes, thus revealing that all selected samples had trace elements not measured by ICP-OES amounting to 0.03± 0.004% of the overall composition (see Note on Results from ICP-MS in Supporting Information). Given the presence of 0.03% additional elements discovered by ICP-MS, each set of measurements were normalized to 99.97% rather than 100%.

Table 2 Elemental compositions for two modern bronzes before normalization

Artist	Accession #	Element in wt.%																					Elemental sum
		Cu		Zn		Sn			Pb	Fe		Ni		As		Bi	Cr		Sb			
		324.75	327.40	206.20	213.86	189.92	242.17	242.95	220.35	238.20	259.94	230.3	231.6	193.7	235.0	223.1	205.6	267.7	217.6	231.1	
Maillol	AIC: 1932.1144a	95 (1)	94 (1)	5.06 (4)	5.41 (2)	1.12 (1)	1.11 (2)	1.10 (2)	0.093 (2)	0.093	0.094	0.045	0.030	0.03	0.02	Trace	None		None	None	100.75
	AIC: 1932.1144b	94.5 (4)	93.7 (4)	5.08 (5)	5.43 (3)	1.09 (2)	1.10 (2)	1.08 (1)	0.089 (4)	0.093	0.094	0.046	0.031	0.06	0.01	None	0.001		Trace	None	100.70
Picasso	AIC: 1957.70a1	78.7 (2)	78.4 (2)	12.6 (4)		3.49 (5)	3.43 (4)	3.39 (5)	0.154 (3)					0.05	0.04	0.01	0.001		0.02	0.01	94.74
	AIC: 1957.70a2	83.4 (6)	82.1 (6)	12.7 (1)	13.6 (1)	3.500 (2)	3.43 (2)	3.40 (1)	0.154 (8)	0.095	0.095	0.032	0.019	0.02	Trace	Trace	Trace		Trace	Trace	99.64
	AIC: 1957.70b	81.2 (1)	80.8 (1)	13.1 (3)		4.00 (7)	3.91 (5)	3.88 (2)	0.235 (2)					0.05	0.06	0.01	None		0.02	0.01	98.37

Measured wavelengths (nm) are shown below the corresponding element. Blanks indicate wavelength values that were not measured. For a complete list of elemental compositions before normalization, see Supporting Information ESM 1

Table 3 Normalized elemental composition (wt.%) for 62 modern bronzes from AIC and PMA, which have been separated according to compositionally similar groups cluster A, cluster B, cluster C, and outliers

Artist	Accession #	Element in wt.%								
		Cu	Zn	Sn	Pb	Fe	Ni	As	Cr	Sb
Cluster A										
Bernard	AIC: 1943.1189	87.0 (1)	9.4 (2)	3.34 (6)	0.093 (2)	0.04	0.01	0.03	Trace	0.02
Bonnard	AIC: 1963.927	82.9 (2)	10.74 (1)	3.84 (2)	2.42 (2)			0.04	None	0.08
Brancusi	PMA: 1967.30.6a,b[a]	82.3 (4)	13.4 (1)	3.61 (5)	0.416 (3)	0.15	0.04	0.04	Trace	0.01
	AIC: 1985.542a,b[a]	82.0 (5)	12.96 (8)	4.45 (6)	0.358 (5)	0.22	0.04	0.03	None	0.02
Degas	PMA: 1954.92.21a,b[a]	81.9 (5)	12.5 (1)	4.02 (2)	1.25 (1)	0.26	0.02	0.05	Trace	0.02
	PMA: 1963.181.82a,b[a]	82.8 (2)	11.71 (8)	4.08 (4)	1.25 (1)	0.06	0.01	Trace	Trace	0.06
Despiau	AIC: 1954.324	84.9 (8)	11.6 (1)	2.94 (5)	0.320 (5)	0.15	0.05	0.02	None	0.02
	AIC: 1950.93	84.8 (1)	11.74 (2)	2.96 (2)	0.289 (5)	0.11	0.05	0.03	None	0.02
Knoop	AIC: 1939.238	82.9 (5)	13.65 (9)	3.27 (4)	0.030 (3)	0.07	0.03	0.00	None	0.02
Matisse	AIC: 1958.16	84.6 (5)	11.0 (1)	2.83 (5)	1.23 (1)	0.11	0.04	0.02	None	0.13
	PMA: 1960.146.1a,b[a]	84.8 (2)	12.91 (6)	2.10 (3)	0.067 (2)	0.05	0.01	0.02	None	0.01
	PMA: 1963.210a,b[a]	84.9 (3)	12.8 (1)	2.07 (2)	0.093 (1)	0.08	0.01	None	Trace	0.01
	AIC: 1992.654	84.26 (5)	12.6 (1)	2.87 (4)	0.070 (2)	0.09	0.02	0.03	None	0.01
Picasso	AIC: 1957.70a[a] (figure)	82.9 (4)	13.2 (3)	3.54 (3)	0.159 (3)	0.10	0.02	0.04	None	0.01
	AIC: 1957.70b (base)	82.32 (9)	13.4 (3)	3.99 (5)	0.239 (2)	0.10	0.02	0.06	None	0.01
	AIC: 1967.683	81.84 (6)	14.2 (2)	3.09 (1)	0.612 (5)	0.12	0.02	0.09	None	0.05
	AIC: 1967.685[a]	85.9 (1)	10.5 (1)	3.00 (5)	0.369 (5)	0.08	0.01	0.02	None	0.05
	AIC: 1967.686	82.5 (1)	14.10 (5)	2.68 (2)	0.504 (2)	0.10	0.02	0.07	None	0.04
	AIC: 1967.687	82.6 (3)	13.5 (1)	3.51 (3)	0.187 (8)	0.09	0.01	0.04	Trace	0.03
	AIC: 1967.688	81.75 (2)	14.3 (3)	3.02 (5)	0.621 (5)	0.10	0.02	0.08	Trace	0.04
	AIC: 1967.689	82.78 (7)	13.7 (2)	3.13 (4)	0.162 (2)	0.12	0.01	0.04	Trace	0.03
	AIC: 1967.690	81.0 (2)	14.26 (9)	3.54 (5)	0.267 (4)	0.76	0.02	0.06	Trace	0.03
Poupelet	AIC: 1927.369a[a]	82.6 (1)	14.1 (2)	3.08 (3)	0.140 (4)	0.05	0.04	0.02	None	None
Renoir	PMA: 1950.92.47a,b[a]	83.5 (2)	13.6 (1)	2.62 (3)	0.144 (2)	0.06	0.02	0.03	Trace	0.02
Cluster B										
Maillol	AIC: 1934.383	92.28 (7)	5.85 (5)	1.58 (2)	0.232 (3)			0.03	None	0.01
	AIC: 1947.86	93.6 (3)	4.56 (3)	1.42 (3)	0.239 (3)	0.09	0.02	Trace	Trace	Trace
	AIC: 1934.384	91.8 (5)	5.99 (1)	1.67 (2)	0.269 (4)	0.19	0.01	Trace	None	0.01
	AIC: 1932.1144a,b[a]	93.4 (7)	5.20 (4)	1.09 (2)	0.092 (2)	0.09	0.03	0.03	Trace	None
	AIC: 1971.779	93.5 (6)	4.60 (6)	1.43 (3)	0.244 (9)	0.09	0.02	Trace	Trace	Trace
Matisse	AIC: 1949.202a (base)	93.7 (2)	4.11 (5)	1.32 (3)	0.70 (1)	0.05	0.03	0.05	None	0.03
	AIC: 1949.202b (figure)	92.5 (2)	4.06 (3)	1.95 (3)	1.150 (7)	0.18	0.03	0.06	None	0.03
	PMA: 1967.030.51a,b[a]	94.2 (3)	3.53 (3)	1.69 (3)	0.098 (3)	0.37	0.03	0.03	Trace	0.01
	AIC: 1932.1145	92.8 (5)	3.86 (3)	2.13 (3)	0.96 (1)	0.14	0.02	0.05	None	0.02
Picasso	AIC: 1967.682[a]	89.9 (5)	6.21 (4)	2.32 (4)	1.35 (2)	0.05	0.02	0.02	None	0.09
	AIC: 1964.193	93.0 (1)	5.78 (2)	1.01 (1)	0.072 (2)	0.03	0.02	0.05	None	0.02
Poupelet	AIC: 1927.366	91.0 (4)	7.01 (4)	1.62 (3)	0.141 (3)	0.10	0.02	0.05	None	Trace
	AIC: 1927.365.2	90.8 (8)	7.11 (4)	1.46 (2)	0.158 (2)	0.31	0.05	0.08	None	0.01
	AIC: 1931.568	93.2 (2)	4.85 (7)	1.29 (2)	0.488 (9)	0.09	0.03	0.05	None	0.01
	AIC: 1927.367	93.89 (8)	3.95 (5)	1.74 (3)	0.283 (5)	0.06	0.01	0.03	None	None
	AIC: 1927.364	93.4 (8)	4.53 (2)	1.64 (2)	0.337 (1)	0.06	0.01	0.00	None	None
Cluster C										
Bourdelle	AIC: 1997.543	95.01 (7)	0.785 (1)	3.95 (5)	0.093 (3)	0.02	0.02	0.09	None	Trace
	AIC: 1950.141	95.1 (1)	1.42 (2)	3.19 (6)	0.080 (5)	0.07	0.02	0.06	None	0.06
	AIC: 1925.255	95.2 (1)	1.06 (2)	3.68 (5)	0.023 (1)			0.03	None	0.01

Table 3 (continued)

Artist	Accession #	Element in wt.%								
		Cu	Zn	Sn	Pb	Fe	Ni	As	Cr	Sb
Daumier	PMA: 1986.26.9a,b[a]	95.7 (3)	0.975 (5)	3.04 (3)	0.097 (1)	0.04	Trace	0.10	Trace	0.02
Orloff	AIC: 1930.227	95.0 (8)	1.32 (1)	3.48 (3)	0.053 (4)	0.04	0.03	0.04	None	Trace
Poupelet	AIC: 1927.368	93.6 (1)	1.89 (1)	3.82 (4)	0.508 (6)	0.07	0.03	0.09	None	0.01
	AIC: 1927.365.1	93.2 (6)	2.08 (2)	3.90 (5)	0.463 (7)	0.17	0.02	0.06	None	0.04
Rodin	PMA: 1967.30.73a,b[a]	94.0 (3)	1.48 (2)	4.29 (8)	0.047 (1)	0.03	0.03	0.09	Trace	0.04
	PMA: 1929.7.4a,b[a]	95.1 (4)	0.74 (1)	3.84 (5)	0.111 (2)	0.02	0.01	0.13	Trace	0.02
Outliers										
Bouraine	AIC: 1973.774	77.9 (2)	20.4 (1)	0.45 (1)	0.87 (1)	0.20	0.04	0.06	None	Trace
Bourdelle	AIC: 1953.168	88.97 (6)	8.1 (1)	2.70 (4)	0.153 (5)			0.07	None	0.02
Daumier	PMA: 1957.127.11a,b[a]	88.6 (4)	8.06 (9)	2.68 (3)	0.351 (9)	0.13	0.06	0.06	Trace	0.05
	PMA: 1986.26.275	88.2 (3)	8.54 (2)	2.96 (4)	0.155 (3)	0.04	0.02	0.02	Trace	0.01
Duchamp-Villon	AIC: 1957.165	75.2 (5)	22.09 (5)	1.35 (2)	1.25 (2)	0.08	0.01	0.01	None	None
Landowski	AIC: 1923.314	85.9 (6)	7.58 (3)	5.39 (7)	0.84 (1)	0.15	0.06	0.05	None	0.04
Lipchitz	AIC: 1996.394	89.6 (1)	5.26 (2)	3.32 (1)	1.290 (6)	0.20	0.11	0.04	Trace	0.18
	AIC: 1943.594	89.1 (1)	3.24 (1)	5.41 (4)	1.88 (2)	0.08	0.14	0.03	None	0.11
	AIC: 1955.826	87.70 (9)	5.66 (6)	3.95 (6)	2.53 (3)			0.04	None	0.10
	PMA: 1949.78.1a,b[a]	86.8 (2)	6.29 (4)	6.24 (5)	0.334 (6)	0.18	0.04	0.07	Trace	0.04
	PMA: 1955.96.2a,b[a]	85.4 (3)	8.8 (1)	5.19 (6)	0.359 (3)	0.13	0.04	0.09	Trace	0.03
Maillol	PMA: 1950.92.44	92.5 (5)	3.16 (1)	2.76 (2)	0.123 (2)	1.32	0.04	0.09	Trace	0.02
Picasso	AIC: 1949.584	91.5 (2)	2.96 (3)	4.90 (8)	0.545 (6)	0.04	0.02	0.03	None	Trace
Poupelet	AIC: 1931.569	62.3 (9)	33.5 (1)	0.74 (1)	2.81 (6)	0.42	0.08	0.05	None	0.04
Zadkine	PMA: 1964.80.1a,b[a]	85.3 (4)	12.8 (1)	0.87 (2)	0.765 (2)	0.15	0.04	0.04	Trace	0.01

Standard deviations of the elemental composition of modern bronzes are indicated by parenthesis. Elemental compositions from two different sites (base and main body of the same sculpture) are shown for Matisse's *The Serf* (AIC: 1949.202a and b) and Picasso's *Flowers in a Vase* (AIC: 1957.70a and b). For both sculptures, the base and main body are believed to have been cast separately and welded together

[a] Value is an average of two measurements

In a few cases (for example, 1985.492a and 1957.70, as indicated in Supporting Information ESM 1), elemental sums before normalization were lower than 95%; this was correlated to incorrect sampling from the sculptures (one sample was scraped rather than drilled) or errors during sample preparation (loss of material during transfer, for example) so that repeating the measurements on drilled samples that were carefully prepared always resolved the problem. Overall, the Cu content of these modern bronze sculptures range from 62.3% to 95.7%, with varying amounts of the two major alloying elements (0.74–33.5% Zn and 0.45–6.24% Sn). Minor alloying elements include 0.02–2.81% Pb, 0.02–1.32% Fe, and 0.004–0.14% Ni with, in some cases, trace amounts of As, Bi, Cr, and Sb as shown in Table 3.

Experimental error, accuracy, and repeatability

In the following paragraphs, some relevant examples are given to illustrate issues that must be taken into account when performing ICP-OES analysis of modern bronze sculptures, including sources of experimental error, sample location, sampling methods, and errors associated with them, as well as accuracy, reproducibility, and use of multiple samples to determine if multicomponent pieces were cast from the same alloy. Accuracy and repeatability of the method were evaluated based on measurements of the standards and comparison with their certified values (see Supporting Information ESM 1).

Replicate samples, obtained either by halving the total amount of material drilled at a single location or by collecting samples from the same sculpture but drilled at different locations, were also analyzed in order to examine the variability of the data due to sample location in the cast or to error associated with ICP-OES measurements but also to answer questions on whether or not sections of complex sculptures were cast together or from different alloys. Measurements were found to be repeatable. For instance, Maillol's *Renoir* (AIC: 1932.1144) provided two samples (a and b) from the same sculpture, where the samples came

from the back (a) and front (b) corners of the bottom edge. Both measurements are within ±0.5 wt.% of each other and are overlapping with one another within their uncertainties, for almost every element measured (see Table 2 and Supporting Information ESM 1). Furthermore, almost every bronze sculpture from the PMA examined here was sampled in two different locations with resulting measurements showing high overlap within their uncertainties (see Supporting Information ESM 1). Duplicate measurements are indicated by superscript letter in Table 3, where the values shown are an average of the two measurements after normalization. Similar results were found for Picasso's *Flowers in a Vase* (1957.70) where samples (a1) and (a2) originated from the underside of the main body and sample (b) came from the underside of the middle of the base plate. After normalization, elemental compositional results from all three samples (a1, a2, and b) are within ±0.6 wt.% of each other indicating that both the main body and the base plate were very likely cast at the same time from the same bronze composition (see Table 3).

Similarly, Matisse's *The Serf* (AIC 1949.202) was sampled from two sites (a: figure, bottom of right foot extension into base and b: base, back right corner of underside) on the sculpture to ascertain whether the main figure and base were cast from the same bronze composition and later joined together (see Fig. 1a, b). As seen in Table 3 and ESM 1, the measurements are within ±1.2 wt. % of each other, indicating that indeed the two sections were most probably cast at the same time using the same bronze composition. Moreover, the data from sites (a) and (b) illustrate the degree of variation in measurements that can be expected due to sample location in the cast and due to error associated with ICP measurements.

Composition clusters

By plotting the ICP-OES-obtained concentrations of the two main alloying elements (Zn and Sn) for all 62 modern bronzes, three different compositional clusters become apparent, as listed in Table 3 and shown in Figs. 2, 3, 4, and 5.[1] These three clusters represent: (A) high-zinc brass (9–16 wt.% Zn; 2–4.5 wt.% Sn), (B) low-zinc brass (3–8 wt.% Zn; 0.75–2.5 wt.% Sn), and (C) tin bronze (0–2.5 wt.% Zn; 2.7 –4.5 wt.% Sn). It is immediately evident that, although copper-based sculptures are invariably identified as bronzes in museum labels and catalogs, from a metallurgical standpoint, only a minority of the sculptures, grouped in cluster C and in its vicinity, can be categorized as bronze alloys, while all the others are brass alloys. Furthermore, these three clusters (A, B, and C) may correlate to specific commercially available copper alloys at the time such as copper alloys 210 (Gilding Metal 95–5% Zn), 226 (Jewelry Bronze 88–12% Zn), 230 (Red Brass 85–15% Zn), 220 (so called "Commercial Bronze" 90–10% Zn), 240 (Low Brass 80–20% Zn), 268 (Yellow Low Brass 65–35% Zn), or 405 (Penny Bronze 96–4% Zn–1% Sn) [2, 31]. These and other recycled alloys may have been added to charges of pure Cu, Zn, Sn, and Pb in an effort to reduce the cost of the sculpture. The latter practice may also explain the presence of intermediate compositions that do not fall within the main clusters.

The clusters encompass not only sculptures with foundry marks but also unmarked sculptures, allowing for speculations that the unmarked sculptures might have been cast at the same foundries that are most represented in these clusters. About one third of the sculptures in this study are marked with the name of the casting foundry. Some hypotheses can also be drawn in terms of the date of production of the sculptures; however, it should be mentioned that generalizations by date are challenging due to the fact that, although many of the model creation dates are known, the casting dates of so many of these sculptures are not known. It was common to wait until there was an actual buyer to have a cast made, so the date of casting of the sculpture could be different from the date of creation of the model. It is only when artist, dealer, or foundry records indicate an order by a particular client, for which the piece can subsequently be identified by its trail of owners (its "provenance"), that it is possible to have a firm casting date for a sculpture.

In the following sections, the compositional clusters that emerged from the elemental analysis of the alloys are discussed in terms of artist, foundries, casting and model fabrication date, and casting method, highlighting the links between material data and art historical parameters.

High-zinc brass (cluster A)

Members of this cluster are listed in Table 3 and plotted in Figs. 2, 3, 4, and 5. A chronological correlation can be made here since castings of the latest creation dates (1929–1957) have relatively high Zn content (above 7.5 wt.%) and thus all fall outside clusters B and C, with most of the sculptures created after World War II (1945–1957) clustered in A. The only exception is Picasso's *Female Figure* (AIC: 1967.682), cast in the mid-1940s, which falls in cluster B. It is possible then that this particular sculpture may have been cast by Valsuani using an earlier alloy composition (i.e., by remelting an earlier sculpture). This change in composition by date reflects the increasing use by artists of foundries

[0] It is important to note that ellipses highlighting the three clusters have been drawn on the figures to simply guide the eye and have no statistical significance. However, given that the plots already give quite clear separations of the groups, statistical analysis was not deemed necessary at this time.

Fig. 1 **a** Front view of Matisse's *The Serf* (AIC: 1949.202) from the Art Institute of Chicago and **b** detailed view of the underside of the same sculpture. The detailed view shows two sampling sites (**a** figure, bottom of right foot extension into base and **b** base, back right corner of underside). Photos courtesy of the Art Institute of Chicago Conservation Laboratory

specializing in lost-wax casting during the first half of the twentieth century. The increased Zn content in the late castings, leading to melting temperature around 1,000 °C, may reflect the desire to cast at lower temperature, given the limited strength of the plaster-based shells used in the lost-wax method before WWII. Most of the lost-wax castings are grouped in this cluster, with good correlation to the C. Valsuani and A.A. Hébrard foundries (see Tables 1 and 3 and Figs. 3 and 5). In fact, 14 out of 18 sculptures with the C. Valsuani foundry mark fall into cluster A. XRF results by Kosinski et al. [4] on 21 sculptures from Matisse and ICP results by Dussubieaux [18] on a subset of eight of the same samples compare well with those described in this work. Ten of the 21 sculptures analyzed by those authors, which were created in the C. Valsuani Foundry from 1929 to 1931, have reported compositions that would group them in cluster A (this work), with three other sculptures in the vicinity of the composition of cluster A.

Three sculptures bearing the mark of the lost-wax casting foundry of A.A. Hébrard (two by Degas, *Woman Rubbing her Back with a Sponge, Torso* (PMA: 1954.92.21) and *Woman Taken Unawares* (PMA: 1963.181.82), and Bernard's *Girl with Pail* (AIC: 1943.1189)) are also within cluster A. The casting dates for these works (Table 1) suggest that this foundry used the same metal composition throughout a relatively long time period (from 1910 to post-1920). Based on Figs. 2, 3, 4, and 5, speculations about the origin of some of the unmarked sculptures can be made. For

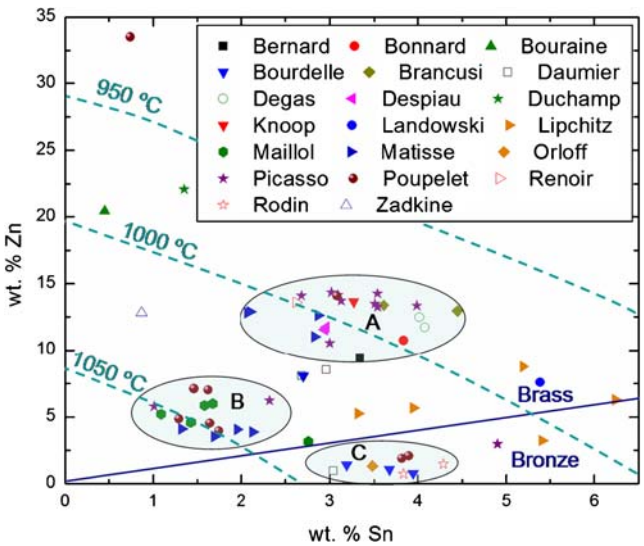

Fig. 2 Elemental composition plot for modern sculptures identified by artist. The three ovals indicate alloy clusters (*A*, *B*, and *C*). *Dashed lines* show melting temperatures corresponding to the Cu–Sn–Zn liquidus lines [1]. The *solid line* marks the compositional difference between brass and bronze, with Zn and Sn, respectively, as the major alloying element

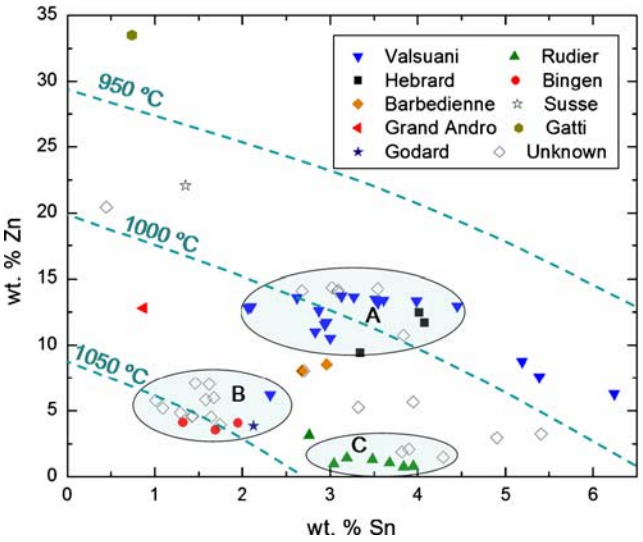

Fig. 3 Elemental composition plot for modern sculptures identified by foundry

example, it is possible to hypothesize that Bonnard's *Spring Frolic* (AIC: 1963.927), grouped with cluster A, might have been cast by the Hébrard or the Valsuani foundry. The tentative date of creation of the work, 1904–1906, suggests that Hébrard may be the more likely foundry of the two, as it began operation in 1902 whereas the Claude Valsuani foundry opened in 1908 [3]. It is also possible that another foundry, not listed here, was using alloys in this same range (9–16 wt.% Zn; 2–4.5 wt.% Sn).

Low-zinc alloys: low-tin brass (Cluster B) and tin bronze (Cluster C)

Low-Zn alloys can be further divided into two subgroups, labeled B and C (see Table 3, Figs. 2, 3, 4, and 5). An alloy composition low in Zinc (below 7.5 wt.%) is characteristic of the majority of casts from models created prior to WWI. This result, for example, points to a creation date prior to WWI for the two sculptures by Poupelet, *Cat* (AIC: 1927.366) and *Goat* (AIC: 1931.568), of unknown creation date, which is also supported by the acquisition dates of 1927 and 1931, respectively (Fig. 4a, b). Furthermore, low-Zn alloys also correlate well with sand cast sculptures, which typically fall into clusters B and C.

Cluster B notably groups two sculptures by Matisse (*The Serf* AIC: 1949.202a (base) and b (figure) produced by sand casting in 1908 (Fig. 1a, b) and *Standing Nude with Arms Raised* PMA: 1967.030.51a, b), which both bear the Bingen-Costenoble foundry mark. Interestingly, in the study performed by Kosinski et al. [4], Matisse's sculpture *The Serf*, known to have also been sand cast by Bingen-Costenoble in 1908, falls into cluster B and exhibits similar composition to *The Serf* in the AIC collection. The differences in metal composition in the two casts of the same model effectively illustrate the spread or breadth of the cluster size between individual castings within a particular foundry. Matisse's *Small Crouching Nude without an Arm* (AIC: 1932.1145), attributed by scholars to the F. Godard foundry [4] and cast perhaps in 1922 or 1923, also falls within cluster B with one of the highest Sn content in that cluster. The compositional data in this study are confirmed by results from four of 21 Matisse's sculptures in the study by Kosinski et al. [4], which are known to have been sand cast in 1922 by the Godard foundry and show compositions that would group them in cluster B (3–8 wt.% Zn; 0.75–2.5 wt.% Sn).

Five out of the six Maillol sculptures presented here are also within cluster B and, based on visual observation, appear to have been sand cast. The PMA version of Maillol's *Leda* (PMA: 1950.92.44), which bears a Rudier foundry mark, has a composition between clusters B and C,

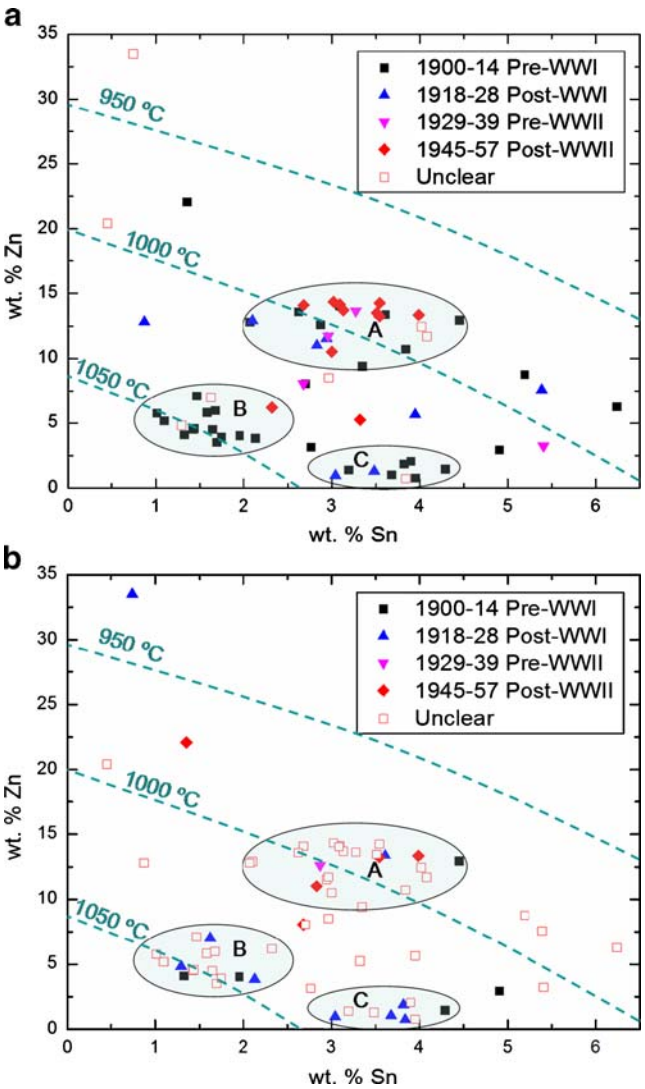

Fig. 4 Elemental composition plot for modern sculptures identified by **a** date of sculpture creation and **b** casting date

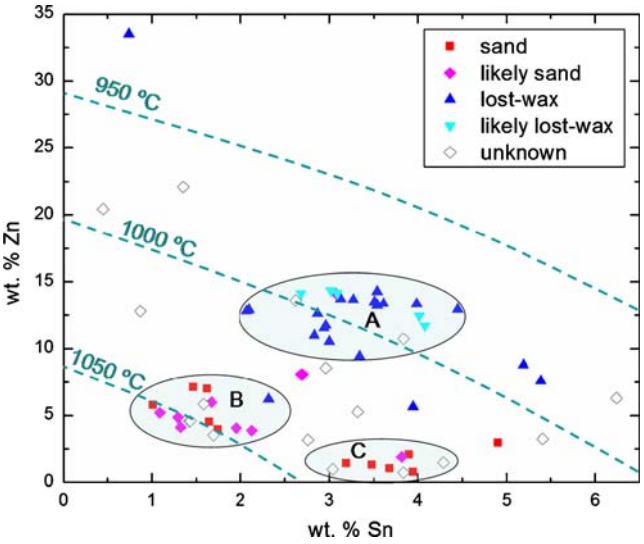

Fig. 5 Elemental composition plot for modern sculptures identified by casting method

with a slightly lower Sn content (2.76 wt.%) and higher Zn content (3.16 wt.%) than other members of cluster C. Interestingly, the AIC version of Maillol's *Leda* (AIC: 1947.86), which is identical in design to the PMA version, is clearly in cluster B and was most likely not cast by the Rudier foundry, given its high Fe content (1.32 wt.%), which is unlike all of the other sculptures cast by the Rudier foundry in this study. Presumably, different versions of the same sculpture were cast in different foundries at different times for unknown reasons (i.e., cost, cast quality, availability of foundry, request by the buyer, unauthorized copy, etc.).

Cluster B also contains two sculptures by Picasso: *Jester* (AIC: 1964.193), which was created in 1905, and *Female Figure* (AIC: 1967.682), which was created circa 1945–1947. Based on visual inspection, *Jester* appears to have been sand cast, which is consistent with other sculptures in this cluster, while *Female Figure* has a Valsuani mark and the physical characteristics of having been lost-wax cast. Compared to other sculptures cast by the Valsuani foundry, this alloy composition is unique and may represent another cluster or may be an anomaly. It is stylistically related to the artist's *Standing Women* series (AIC: 1967.683-690), all of which can be found in cluster A and some of which bear the Valsuani mark.

Cluster C show good correlation with the Alexis Rudier foundry. In fact, six out of seven sculptures with the Alexis Rudier foundry mark fall into cluster C, with the exception of Maillol's *Leda* (PMA: 1950.92.44) as discussed in the above paragraph. Rodin also used the Rudier foundry (in addition to many others) as illustrated here by his *The Athlete* (PMA: 1929.7.4), which was cast in 1925 and stamped with the Rudier foundry mark. An earlier version of *The Athlete* (PMA: 1967.30.73), which was cast in 1904, has a composition very similar to the 1925 cast. It is thus likely that the 1904 version was also cast in the Rudier foundry. This study highlights that, although the dates for the two sculptures span two decades (from 1904 to 1925), the composition used by the Rudier foundry does not seem to have changed substantially. Previous studies with EDX and proton-induced X-ray emission on six Rodin sculptures cast at the Rudier foundry between 1880 and 1920 [20] showed values of 3.6% Sn and 1.3% Zn which are well within the ranges of cluster C in this study (3–4%Sn and 0–2% Zn) where all the Rudier cast sculptures are grouped. An additional sculpture by Laurier cast before 1927 also by Rudier and discussed by Selwyn et al. [21] has a reported alloy composition with 4% Sn and 1% Zn which also falls into cluster C.

Also, within cluster C, two unmarked sculptures by Poupelet (*Cock*: AIC: 1927.368 and *Peasant*: AIC: 1927.365.1) appear very likely to have been sand cast at the Rudier foundry. One would expect that the companion piece, Poupelet's *Cow* (AIC: 1927.365.2), to Poupelet's *Peasant* (AIC: 1927.365.1) would also have the same composition; however, the composition of the *Cow*, which is at present attached to the *Peasant* by a bronze "rope," is clearly in cluster B and was most likely not cast by Rudier. Four other sculptures by Poupelet are found in cluster B. This suggests that Poupelet's *Cow* and *Peasant* may have been originally conceived of separately and/or cast at different times and coupled later. Although less likely, it is also possible that a different alloy was chosen based on the appearance of a desired patina. It was not uncommon for the artists of the first half of the twentieth century to use a number of foundries, depending on the type of work, its intended market, and the commission [32].

Outliers

As illustrated in Table 3 and Figs. 2, 3, 4, and 5, many of the sculptures analyzed here fit into one of the three clusters (A, B, or C); however, a number of outliers exist and they will be discussed here. For example, Bouraine's *Dancing Woman with Hoop* (AIC: 1973.774c) is very different from all other modern bronzes presented here since it has a very low amount of Sn (0.45 wt.%) and relatively large amounts of Zn (20.4 wt.%) and Pb (0.87 wt.%). It is important to note that a detachable hoop element of this sculpture was left unpatinated, so that the color of the alloy is evident, which may have been a reason to choose a very brassy (high Zn) composition (though the figure itself is patinated).

Similar in composition to Bouraine's *Dancing Woman with Hoop* (AIC: 1973.774), Duchamp-Villon's *Horse* (AIC: 1957.165) also has a low amount of Sn (1.35 wt.%) and large amounts of Zn (22.09 wt.%) and Pb (1.25 wt.%). Furthermore, Duchamp-Villon's *Horse* is the only sculpture

here with a Susse foundry mark. Another sculpture with a unique foundry mark and alloy composition is Poupelet's *Cat* (AIC: 1931.569), a lost-wax cast with an L. Gatti foundry mark, which is well outside of all three clusters and has the highest Zn content (33.5 wt.%), resulting in the lowest liquidus temperature. It also has the highest Pb content (2.81 wt.%), second highest Fe content (0.42 wt.%), third highest Ni content (0.08 wt.%), and second lowest Sn content (0.74 wt.%) within the data presented here.

Zadkine's *Harlequin* (PMA: 1964.80.1a, b) is relatively high in Zn (12.8 wt.%) and low in Sn (0.87 wt.%) and is the only sculpture presented here from the Grandhomme-Andro foundry. It is possible that this composition is typical of that used by the Grandhomme-Andro foundry, although more sculptures from this foundry need to be examined to confirm this supposition. Furthermore, the fact that three individual examples of foundries (Grandhomme-Andro, Susse, and L. Gatti) have clearly distinct Zn and Sn compositions, as compared to the other foundries, suggests that composition is well correlated with the foundry responsible for the casting. However, more examples from these underrepresented groups should be studied before this hypothesis can be confirmed.

Three of Lipchitz's sculptures including *Rape of Europa* (AIC: 1943.594), *Sailor with Guitar* (PMA: 1949.78.1a,b), and *Woman with Braid* (PMA: 1955.96.2a, b) have relatively high Sn content (5.41, 6.24, and 5.19 wt.% Sn, respectively). Interestingly, none of the five sculptures by Lipchitz are within a cluster. Lipchitz's *The Reader* (AIC: 1955.826) and *Mother and Child* (AIC: 1996.394) lie between clusters A and C. These unusual bronze compositions from Lipchitz may not be surprising. Although some of his sculptures were cast in Paris before WWII, he fled in 1941 to the USA, where he remained for the rest of his life. After WWII, Lipchitz had some of his works that he left behind in Paris shipped to the USA, where he cast many of them at the Modern Art Foundry in New York [33]. This may explain at least Lipchitz's *Mother and Child*, which is known to have been cast in the USA. Moreover, *Mother and Child* (AIC: 1996.394), *Rape of Europa* (AIC: 1943.594), and *The Reader* (AIC: 1955.826) all have relatively high Pb content as compared to *Sailor with Guitar* (PMA: 1949.78.1a,b) and *Woman with Braid* (PMA: 1955.96.2a,b), which are known to have been cast by Valsuani, thus suggesting that they may have been cast elsewhere. Three of Matisse's sculptures, which are known to have been cast by the Valsuani foundry in either 1925 or 1929 in the study by Kosinski et al. [4], fall outside of the three clusters presented here due to their high Sn content (5–8 wt.%) and moderate Zn content (4–7 wt.%). This correlates well with three other sculptures (Landowski's *Henry Harrison Getty* AIC: 1923.314 and Lipchitz's PMA: 1949.78.1a,b and PMA: 1955.96.2a,b) examined here and also cast by Valsuani, which have similar Sn (5–6.5 wt.%) and Zn (7–8 wt.%) contents. Based on these observations, it is possible to put forth the hypothesis that another cluster representing another alloy used by the Valsuani foundry exists. Only acquisitions of more examples and data points will allow confirmation of this hypothesis.

Of the four sculptures by Bourdelle with creation dates between 1900 and 1911, three are known to have been sand cast in the Rudier foundry (cluster C) and one, the sand cast and unmarked *Penelope* (AIC: 1953.168), lies between clusters A and B. Although known to have used the Rudier and Susse foundries extensively, Bourdelle also used other foundries, including the sand casting foundries of Godard and of Hohwiller; *Penelope* may have been the product of one of these other foundries [32].

Two sculptures by Daumier (*Alexandre-Simon Pataille* PMA: 1957.127.11 and *L'Obsequieux* PMA: 1986.26.275), which bear Barbedienne foundry marks, are of similar composition to Bourdelle's *Penelope* and fall between clusters A and B, being low in Zn as compared to cluster A and high in Sn as compared to cluster B. Considering that Bourdelle had worked during this period with Rodin, who was known to have used the Barbedienne foundry, it is quite possible that Bourdelle's *Penelope* was cast in the Barbedienne foundry as well. Based on our results, it is possible to speculate that Daumier's *Alexandre-Simon Pataille* and *L'Obsequieux* and Bourdelle's *Penelope*, which have compositions between cluster A and B, may be representative of another cluster corresponding to the Barbedienne foundry.

Conclusions

Using ICP-OES, the metal composition of 62 important modern bronze sculptures was accurately measured, thus presenting a detailed picture of the casting alloys employed at Parisian art foundries in the first half of the twentieth century. Considering the two main alloying elements (Zn and Sn), it is possible to identify three compositional clusters: (A) high-zinc brass, (B) low-zinc brass, and (C) tin bronze with very low zinc. These clusters show correlations to artist, foundry, date, and casting method, providing clues to the attribution of some of the sculptures that do not bear a foundry mark or whose casting date or method are uncertain. In general, the metal composition is determined by the foundry and this generalization seems to be correlated to the casting technology, influenced, in turn, by the reemergence and technical advances of the lost-wax method that occurred in the 1930s.

One quarter of the bronzes studied here fall outside of the identified clusters, which may be due to several factors: (1) additional clusters exist, possibly linked to specific

foundries, but are not identified here due to the limited number of sculptures belonging to these clusters; (2) the artists may have requested a particular metal composition to produce some desired visual effect (metal color, patina); (3) for economic reasons, scrap metal with less well-controlled compositions may have been used.

In summary, the present study constitutes a solid foundation, allowing speculations about the foundry, date, and casting method of an artist's specific sculpture; however, analysis of more sculptures is needed to dissipate some of the ambiguities and open questions that are still present.

Acknowledgements This research benefited from the financial support of the Andrew W. Mellon Foundation. The authors thank Juris Sarins (SIPI Metals Corporation) and Phil Meehan (Atlas Bronze) for providing bronze reference materials and Saman Shafaie and Keith Macrenaris (Northwestern University) for numerous useful discussions. A portion of this work was completed at the Northwestern University Analytical Services Laboratory (NU-ASL). A description of the facility and full funding disclosure can be found at http://pyrite.chem.northwestern.edu/analyticalserviceslab/asl.htm.

References

1. Chang YA, Neumann JP, Mikula A, Goldberg D (1979) Phase diagrams and thermodynamic properties of ternary copper-metal systems. International Copper Research Association, New York
2. Baker H, Benjamin D, Unterweiser PM (1979) Metals handbook: properties and selection: nonferrous alloys and pure metals, vol 2, 9th edn. ASM International, Metals Park
3. Lebon É (2003) Dictionnaire des fondeurs de bronze d'art: France 1890–1950. Marjon Editions, Perth
4. Kosinski D, Boulton A, Nash S, Shell O (2007) Matisse: painter as sculptor. Yale University Press, New Haven
5. Shapiro ME (1981) Cast and recast: the sculpture of Frederic Remington. Smithsonian Institution Press, Washington, DC
6. Debonliez G, Malepeyre F (1887) Nouveau manual complet du bronzage des metaux et du platre. Chez Leonce Laget, Paris
7. Levy TE, Adams RB, Hauptmann A, Prange M, Schmitt-Strecker S, Najjar M (2002) Early bronze age metallurgy: a newly discovered copper manufactory in southern Jordan. Antiquity 76:425
8. Nissen HJ (2003) Uruk and the formation of the city. Yale University Press, New Haven
9. Roy A, Smith P (eds) (2004) Modern art, new museums: contributions to the IIC Bilbao Congress. The International Institute for Conservation, London
10. Learner TJS, Smithen P, Krueger JW, Schilling MR (eds) (2004) Modern paintings uncovered. Modern paintings uncovered symposium. Getty Conservation Institute, London, p 32
11. Learner TJS (2005) Analysis of modern paints. Getty Conservation Institute, Los Angeles
12. Learner TJS, Crook J (2000) The impact of modern paints. Tate, London
13. Rogerson C, Garside P (eds) (2006) The future of the 20th century: collecting, interpreting and conserving modern materials. Archetype, London
14. Grattan DW (ed) (1991) Saving the twentieth century: the conservation of modern materials. Symposium '91: saving the twentieth century. Canadian Conservation Institute, Ottawa, p 440
15. From marble to chocolate (1995) Conservation of modern sculpture. Archetype, London
16. Scott DA (2002) Copper and bronze in art: corrosion, colorants, and conservation. Getty Publications, Los Angeles
17. Singer MC, Fletcher V (2004) The conservation of art's bronzes: preserving the sculpture's history or the artist's intent?. International Institute for Conservation of Historic and Artistic Works, Bilbao
18. Dussubieux L (2007) Laser ablation-inductively coupled plasma-mass spectrometry analysis of ancient copper alloy artifacts. In: Glascock MD, Speakman RJ, Popelka-Filcoff RS (eds) Archaeological chemistry: analytical techniques and archaeological interpretation. American Chemical Society, Washington, DC
19. Selwyn LS, Binnie NE, Poitras J, Laver ME, Downham DA (1996) Outdoor bronze statues: analysis of metal and surface samples. Stud Conserv 41:205
20. Robbiola L, Hurtel L-P (1991) Nouvelle contribution à l'étude des mécanismes de corrosion des bronzes de plein air: caractérisation de l'altération de bronzes de Rodin. Mémoires et Études Scientifiques Revue de Métallurgie 12:809
21. Bourgarit D, Mille B (2003) The elemental analysis of ancient copper-based artefacts by inductively-coupled-plasma atomic-emission spectrometry: an optimized methodology reveals some secrets of the Vix crater. Meas Sci Technol 14:1538
22. Giumlia-Mair A, Keall EJ, Shugar AN, Stock S (2002) Investigation of a copper-based hoard from the megalithic site of Al-Midamman, Yemen: an interdisciplinary approach. J Archaeol Sci 29:195
23. Giumlia-Mair A, Keall EJ, Stock S, Shugar AN (2000) Copper-based implements of a newly identified culture in Yemen. J Cult Herit 1:37
24. Segal I, Kloner A, Brenner IB (1994) Multielement analysis of archaeological bronze objects using inductively coupled plasma emission spectrometry: aspects of sample preparation and line selection. J Anal At Spectrom 9:737
25. Segal I, Rosen SA (2005) Copper among the nomads: early bronze age copper objects from the camel site, central Negev, Israel. Institute for Archaeo-Metallurgical Studies 25:3
26. Tykot RH, Young SMM (1996) Archaeological applications of ICP-mass spectrometry. In: Orna MV (ed) Archaeological chemistry. Organic, inorganic, and biochemical analysis. ACS Symposium Series, Washington, DC, p 625
27. Young SMM, Budd P, Haggerty R, Pollard AM (1997) Inductively coupled plasma-mass spectrometry for the analysis of ancient metals. Archaeometry 39:379
28. Alcock NW (1993) Flame, flameless, and plasma spectroscopy. Anal Chem 67:503R
29. Hill SJ (2007) Inductively coupled plasma spectrometry and its applications. Wiley-Blackwell, New York
30. Pollard AM, Heron C (2008) Archaeological chemistry. The Royal Society of Chemistry, Cambridge
31. Davis JR (2001) ASM specialty handbook: copper and copper alloys. ASM International, Russell Township
32. Curtis P (1995) The hierarchy of the sculptor's workshop: the practice of Emile-Antoine Bourdelle (1861–1929). Archetype, London
33. Wilkinson AG (2000) The sculptures of Jacques Lipchitz: catalogue raisonne. Thames & Hudson, London